First analysis of a Numerical Benchmark for 2D Columnar Solidification of Binary Alloys

E. Arquis[7] - M. Bellet[2] - H. Combeau[1] – Y. Fautrelle[3] – D. Gobin[4] – O. Budenkova[3] – B. Dussoubs[1] – Y. Duterrail[3] – A. Kumar[1] – S. Mosbah[1] – M. Rady[5] – C.A. Gandin[2]– B. Goyeau[6] – M. Založnik[1]

[1] Institut Jean Lamour - *CNRS – Nancy-Université – UPV-Metz, 54042 Nancy cedex, France*
[2] CEMEF - *CNRS – Mines-ParisTech, 06904 Sophia Antipolis cedex, France*
[3] SIMAP - *CNRS – INPG – Université Joseph Fourier, 38402 St Martin d'Hères cedex, France*
[4] FAST - *CNRS – Université Pierre et Marie Curie, 91405 Orsay cedex, France*
[5] *BENHA Institut – Benha / Cairo, Egypt*
[6] EM2C - *CNRS – Ecole Centrale Paris, Grande Voie des Vignes ,92295 Châtenay-Malabry, France*
[7] I2M/TREFLE - *CNRS – Université de Bordeaux – ENSAM-ParisTech – ENSCPB, 33607 Pessac cedex, France*

Please first of all note that this communication is more an invitation for foreign contributors to join this "french" benchmark exercise than a pure scientific paper with fully new matter. We presented very similar calls and matter in previous events in France (CFM Marseille and SFT Le Touquet, MATERIAUX Nantes, Congresses) or outside (MCWASP Vancouver, TMS Symp.,, EUROMAT Glasgow).

Abstract

During the solidification of metal alloys, chemical heterogeneities at the product scale (macro-segregation) develop. Numerical simulation tools are beginning to appear in the industry, however their predictive capabilities are still limited. We present a numerical benchmark exercise treating the performance of models in the prediction of macrosegregation. In a first stage we defined a "minimal" (i.e. maximally simplified) solidification model, describing the coupling of the solidification of a binary alloy and of the transport phenomena (heat, solute transport and fluid flow) that lead to macrosegregation in a fully columnar ingot with a fixed solid phase. This model is solved by four different numerical codes, employing different numerical methods (FVM and FEM) and various solution schemes. We compare the predictions of the evolution of macrosegregation in a small (10×6 cm) ingot of Sn-10wt%Pb alloys. Further, we present the sensitivities concerning the prediction of instabilities leading to banded channel mesosegregations.

KEY-WORDS : *Solidification – Binary Alloys – Mushy region – Numerical Simulation – Macrosegregation*

Introduction

One of the principal challenges of the solidification stage in metal processing is the control of structural and chemical heterogeneities at the product scale – macrosegregations. These defects can critically alter the final product properties and quality. Numerical simulation can be an important tool of progress in process control to mitigate these defects. Nevertheless, at the present development level of simulation codes we still do not have reliable prediction tools. The complexity of the prediction of macrosegregation is a consequence of the fact that the macrosegregation results from the entire history of the strongly coupled processes of heat and mass transfer from the liquid state up to the end of solidification. It depends particularly on the structuring of the phase-change zone (mushy zone) and the relative motion of the solid and liquid phases. Temperature and composition gradients in the liquid induce fluid flow driven by thermal and solutal natural convection. These phenomena are in a strongly nonlinear and delicate coupling, especially in liquid metals, where the disparity of diffusion scales of heat, momentum and mass is particularly large (characterized by very low Prandtl numbers of the order of 10^{-2} and very high Lewis numbers of the order of 10^{4}). Certain transport properties, essential for a good prediction performance of the models, are still poorly characterized. Foremost, the description of the permeability of the porous solid matrix in the mushy zone. The present work is a part of the SMACS project1, the objective of which is to develop better predictive capabilities of macrosegregation models. The methodology on the way there is twofold, following the verification & validation paradigm [1]. On the one hand, we analyze the accuracy performance of numerical models in the prediction of macrosegregation and thermal and solutal natural convection and try to provide numerical benchmark reference results. On the other hand, we perform carefully controlled experiments, to obtain reference results that can be used as a benchmark to characterize the predictive capabilities of the models. This communication presents a part of the results of the SMACS project: the comparison of numerical simulation results for a reference case of solidification of a binary Sn-10 wt%Pb alloy. It is a continuation of the publication of the first series of

results published in [2] that was obtained for the same geometry, but for a Pb-18 wt%Sn alloy.

1. Test-case presentation

The solidifying ingot is contained in a two-dimensional rectangular mold of 0.10m width and 0.06m height, which is shown in Fig. 1. The mold is initially filled with a quiescent and homogeneous liquid Sn-10 wt%Pb alloy at the liquidus temperature corresponding to the initial composition ($T0$ = 219.14 °C). The task is to simulate the solidification of this alloy, considering that the mold is cooled symmetrically by a Fourier boundary condition, identical on both vertical walls, with a uniform and imposed heat transfer coefficient and chill temperature. The top and bottom walls are adiabatic. We suppose a no-slip condition for the velocity of the liquid on all mold walls. Due to the symmetry of the geometry we assume a symmetry of the solution and we hence solve the problem on a half of the full mold geometry.

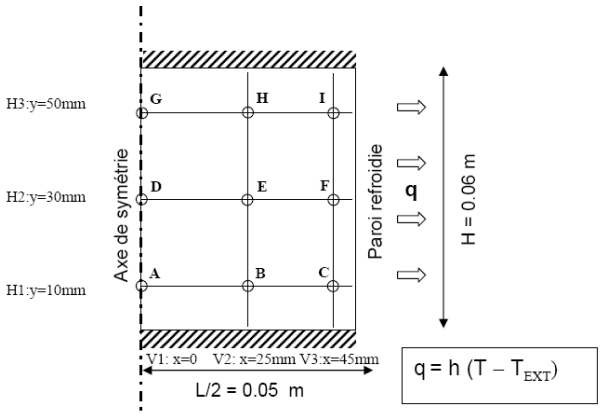

Figure 1: Schematics of the problem

At this stage of the comparison exercise we want to characterize the performance of the numerical solution methods. Therefore, the model describing the solidification was imposed, so that each contributor solves the same equation system. The conservation equations for heat, mass, momentum and solute mass (Eqs. (1–4)) were established by the volume averaging method and are given in Table I.
The microsegregation model corresponds to the assumption of a full thermodynamic equilibrium of the solid and liquid phases – lever rule – Eq. (5). The density of the liquid phase in the buoyancy term follows a linear variation with the temperature and the solute concentration, Eq. (6). The permeability of the porous mushy zone depends on the liquid fraction and the secondary dendrite arm spacing λ_2, which is a fixed parameter, and follows the Kozeny-Carman law, Eq. (7). The detailed specification of the test configuration, the full set of thermophysical parameters, as well as the specifications of the output data are given in Bellet et al. [3] and are published on the website of the benchmark project:

http://www.ijl.nancy-universite.fr/benchmark-solidification.

Momentum	$\nabla\cdot(\mu_l\nabla\mathbf{V}) - g_l\nabla p - \frac{\mu_l g_l}{K}\mathbf{V} + g_l\tilde{\rho}\mathbf{g} = \rho_0\frac{\partial\mathbf{V}}{\partial t} + \frac{\rho_0}{g_l}(\nabla\mathbf{V})\mathbf{V}$	(1)
Mass	$\nabla\cdot\mathbf{V} = 0$	(2)
Energy	$\rho_0\frac{\partial\langle h\rangle}{\partial t} + \rho_0 c_p\nabla T\cdot\mathbf{V} - \nabla\cdot(k\nabla T) = 0$	(3)
Solute	$\frac{\partial\langle C\rangle}{\partial t} + \nabla C_l\cdot\mathbf{V} = 0$	(4)

Therrmodyna equilibrium	$\langle C\rangle = g_l C_l + g_s C_s = \left(g_l + k_P(1-g_l)\right)C_l$ $T = T_m + mC_l$	(5)
Density dependance	$\tilde{\rho} = \rho_0(1 - \beta_T(T-T_0) - \beta_c(C_l-C_0))$	(6)
Permeability law	$K = \frac{\lambda_2^2 g_l^3}{180(1-g_l)^2}$	(7)

2. General description of the solidification process

Before presenting the comparison of the results, we will show the evolution of the solidification on the example of one of the simulations. Figure 2 shows the solute concentration at two different stages of the solidification, t = 40 s and t = 120 s.

We can see that the main features of the macro-segregation develop early through the solidification process. After a time t of about 100 s the principal characteristics can be recognized: a positive segregation band along the symmetry axis (left boundary), a negative segregation pocket in the upper central part of the ingot, and the formation of channel segregates, inclined at about 45°, in the bottom central part. The time evolution of the liquid fraction and of the average concentration in point E, shown in Fig. 2(b), however shows that the macrosegregation continues to evolve even up to small liquid fractions (approximately until g_l = 0.3).

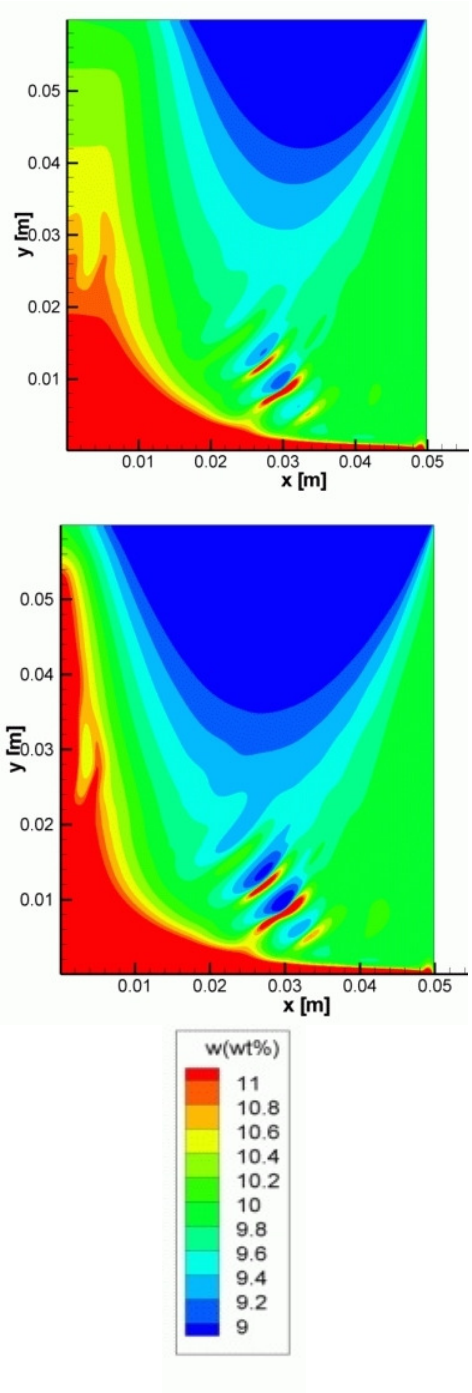

Figure 2 – Concentration maps at t = 120 s (top) and t = 600 s (bottom).

Observing the beginning of solidification, we can see that the channels in the mushy zone start to form very early, in a zone where the convective flow is particularly intense (Fig. 3(a) showing the situation at t = 40 s). The flow here is driven by the thermal convection, which is induced by the thermal gradient between the cooled wall on the right and the hot liquid on the left, and drives the flow in a clockwise direction. On the other hand, the solute rejection into the liquid, a consequence of the solidification, causes a lead enrichment of the liquid in the mushy zone. This creates an additional buoyancy gradient that drives the flow in the same sense as the thermal buoyancy. The cooperating thermal and solutal forces induce a flow circulation in the fully liquid zone, which is shown in Fig. 3(a) together with the liquid fractions in the mushy zone. The latter already show an onset of a destabilization in the bottom zone that starts to develop into channels. A horizontal channel is also formed along the bottom wall. The formation of these channels is related to the flow direction of the liquid. The solute enrichment caused by the flow of enriched liquid from the interior of the mushy zone into the bulk liquid zone induces a local delay of solidification and the formation of channels in the mushy zone. The re-build-up of the flow that now passes preferentially through the channels, due to their lower hydrodynamic resistance, creates a positive segregation in the channels. At t = 120 s the channels are well developed, as shown in Fig. 3(b). The liquid fraction in the channels is now 0.99, while it is of the order of 0.5 in their vicinity. As solidification continues, the channel segregates and the positive segregation band at the left boundary develop until the final macrosegregation, shown in Fig 5.

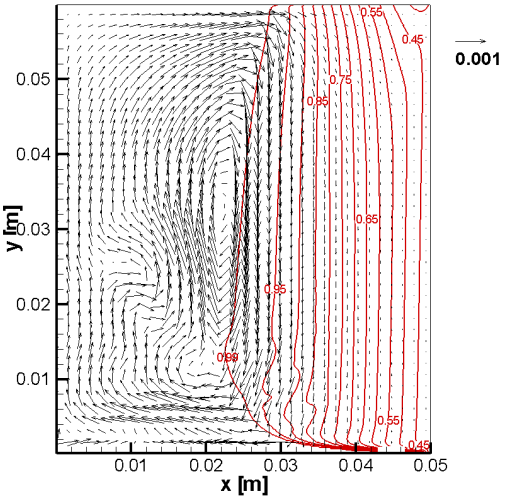

(a)

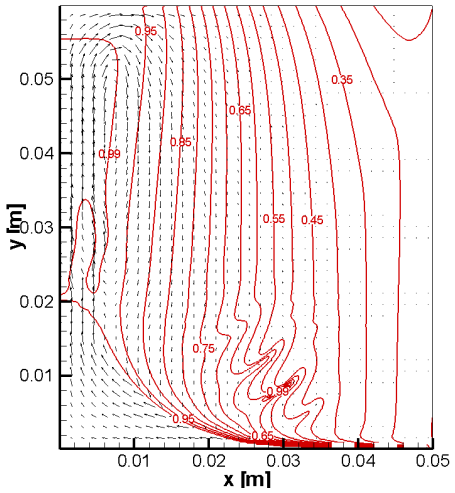

(b)

Figure 3: Evolution of solidification and flow: velocity field (vectors, the size scale in m/s is indicated with a norm vector) and liquid fraction iso-lines at 40 s (a) and 120 s (b)

What the dynamics of solidification is concerned, the evolution of both the liquid fraction and concentration at certain locations (points A, B, E, H and I, see figure 1 for corresponding coordinates) presented in Figure 4 show that even the solidification last about until 450 s, the composition exhibits a relatively stable evolution from 200 s. The sudden decrease in liquid fraction corresponds to the formation of eutectic. Following the lever rule hypothesis, due to the value of 10% for the initial mass composition in Pb, 21% of solid shuld appear at the eutectic. Note that due to the variation in local solute concentration, the phase rate formed at eutectic varies itself: at point A for instance, it is greater than 40%, while at point I it is lower than 10%.

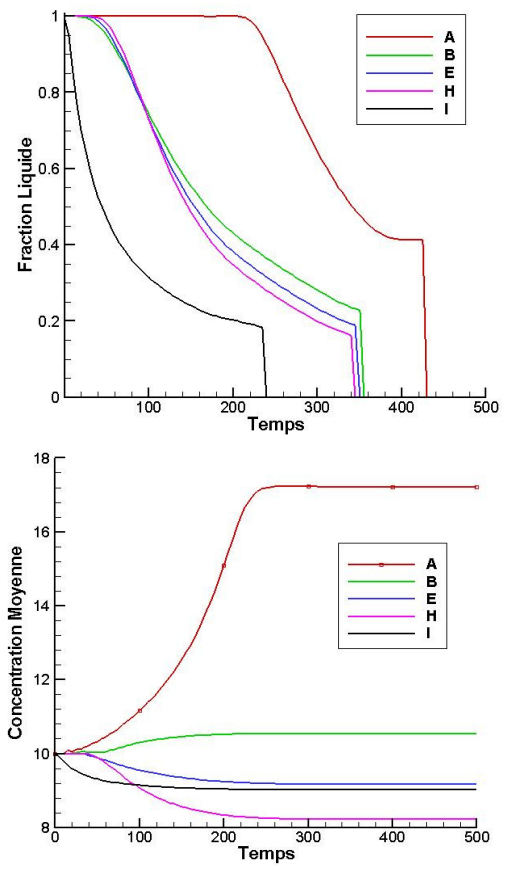

Figure 4 – Time evolutions of liquid fraction (top) and concentration (bottom) at different points A, B, E, H and I of the cavity

3. Comparison of numerical solutions

The objective of this communication is to present the results obtained by four groups with four independent computational codes. One of the codes is based on the finite element method and was developed by CEMEF (R2Sol) [4]. The other three codes use the finite volume method.

(a) *R2Sol*, developed in CEMEF [5];
(b) a code developed with the commercial software *FluentTM6.2* in EPM-SIMAP [6];
(c) *Solid*, developed in Institut Jean Lamour (IJL) [7];
(d) *Thetis*, developed in TREFLE [8].

In codes (b) and (d) the heat conservation equation is solved in the temperature formulation, while in codes (a) and (c) it is solved in the enthalpy formulation, with the average enthalpy $\langle h \rangle$ as the leading variable [6]. In codes (a), (c) and (d) the solute conservation equation is solved in terms of the average concentration $\langle C \rangle$ and the coupling with the phase change is done according to the scheme proposed by Voller [10]. In code (b) the solute conservation is solved for each phase (solid and liquid) separately, employing two equations, one for each phase. The discretization of the convective terms is done by a 2nd or higher order scheme in codes (b) (QUICK) and (d) (TVD) [9]. Code (c) uses a 1st order upwind scheme and code(a) a SUPG scheme, stabilized by a supplementary diffusive term in equation (4).

Institutions	Sofware (transport terms scheme)	Grid (min mesh size (m))	Time step (s)
CEMEF (a)	R2SOL EF (SUPG)	5763 nœuds ($2{,}5\ 10^{-4}$)	$5\ 10^{-3}$
EPM (b)	FLUENT VF (Quick)	200 x 240 ($7{,}14\ 10^{-4}$)	$5\ 10^{-3}$
IJL (c)	SOLID VF (Upwind)	275 x 328 ($1{,}9\ 10^{-4}$)	$5\ 10^{-3}$
TREFLE (d)	THETIS VF (TVD)	268 x 324 ($1{,}9\ 10^{-4}$)	$1\ 10^{-3}$

Table I : some main characteristics of the sofware used for this comparison exercise (scheme, mesh, time-step)

The characteristics of the mesh and the time step used by the four contributions are reported in Table I. A mesh and time step sensibility study was conducted by each contributor. While all details of these studies cannot be presented here, the most

important observations are summarized. The mesh convergence observed with respect to the maximum and minimum values of the solute concentration after completed solidification is shown in Fig. 4. The four codes show very similar sensibilities of the maximum value of the average concentration at the end of solidification to the mesh density. In all cases this value clearly approaches the theoretical limit of the maximum concentration – the eutectic concentration ($C_{eut} - C_0)/C_0$ = 2.81) – with an order of convergence smaller than one. Note that code (b) does not account for the eutectic reaction and thus allows a maximum concentration higher that the eutectic. Except for code (a) the sensibility of the minimum value to the mesh size is very weak and does not reach the minimum theoretical value ($k_p C_0 - C_0)/C_0$ = –0.93).

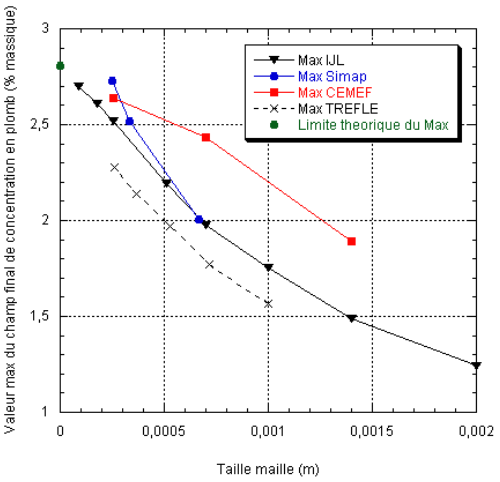

(a)

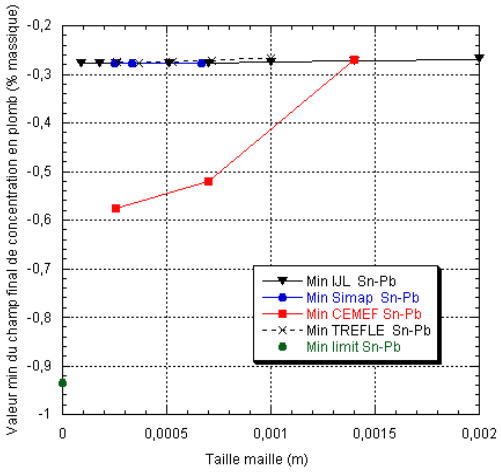

(b)

Figure 4: Mesh convergence of the averaged relative segregation (C–C0 in wt%Pb) at the end of solidification: (a) maximum of the field, (b) minimum of the field

4. Analysis of the results

Concentration field

Maps of the average concentration field at the end of solidification (t = 600 s) obtained by the four contributors are presented in Fig. 5. The macrosegregation is in accordance with the description in the previous section and the four simulations are in qualitative agreement on the general macrosegregation map. The principal differences are however:

1. the extent of the positive macrosegregation zone in the vicinity of the symmetry plane (left boundary), where the simulation (c) shows a zone less enriched in lead at the mid-height in this region;
2. the position and the number of channel segregates, which are virtually nonexistent in simulation (a) and are weaker in simulation (d) than in (b) and (c).

Comparisons of the concentration profiles along horizontal sections H1, H2 et H3 and vertical sections V1, V2, V3 (not shown in this communication) show that the values are very close in all simulations, except in the aforementioned zones on the left as well as in and around the channels.

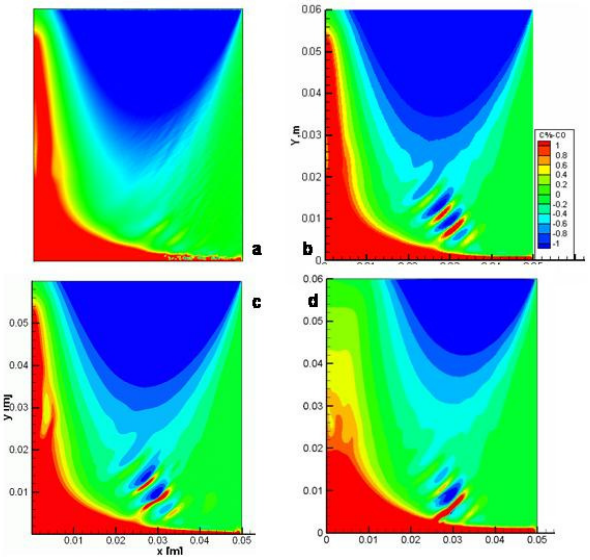

Figure 5: Final maps of segregation ($C - C_0$ in wt%Pb) obtained by the four contributors

Flow velocities

An important element of comparison of the solutions is the velocity field in the liquid. Figure 6(a) shows the profile of the velocity magnitude in the horizontal mid-plane (H2) at t = 120 s. These velocities are relatively weak (< 1 mm/s). We can note a very good agreement of the solutions in the right part of the profile, which corresponds to the mushy zone with

liquid fractions smaller than 0.98. The dispersion of the solutions is very large, however, in the left part, corresponding to high liquid fractions ($0.98 < g_l \leq 1$). We have to note that the temperature and liquid fraction profiles are similar for the four contributions. In Fig. 6(b) we show the evolution of the velocity magnitude in point E (midpoint of profile H2) with time. All solutions predict overall the same evolution, with two peaks that occur at the same times. We find a good agreement of the solutions with some notable differences in the beginning, until about $t = 30$ s. This initial interval corresponds to the period when liquid fractions were high.

As a summary of the analysis of the different details of the four solutions, we can say that the principal differences in terms of macrosegregation are found in two parts of the ingot: in the central zone (left boundary of the domain) and in the channel segregates. These are the zones most affected by the transport at high liquid fractions, where we generally observed the biggest differences between the solutions in terms of flow velocities. The central zone solidifies last and stays at high liquid fractions for the longest time. The channels also form at high liquid fractions. Hence, it is possible to attribute the differences observed in macrosegregation to differences in the solutions at high liquid fractions.

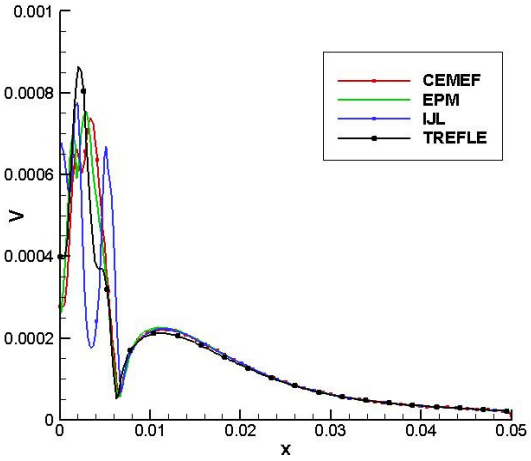

(a)

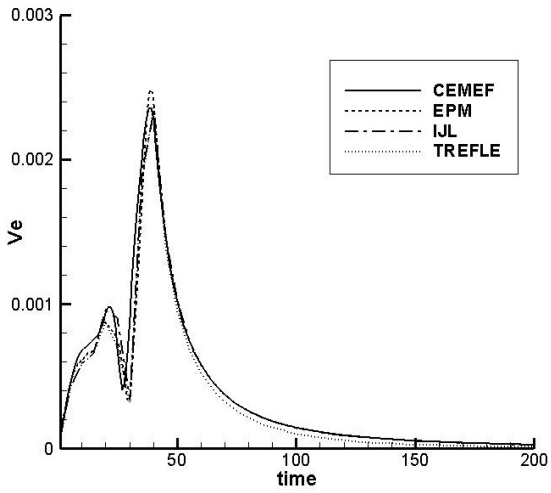

(b)

Figure 6: Comparison of velocities a) Profiles of the velocity magnitude ($|\vec{v}|$) in the horizontal mid-plane (H2) at t = 120 s (b) Time evolutions of the velocity magnitude ($|\vec{v}|$) in point E (mid-point of the profile H2).

Conclusion

This communication presents the first results of the comparison between different numerical procedures in the solution of an identical “minimal” solidification model. More detailed analyses of the convergence of the solutions and of the reasons behind the differences that we found are still required. However, we can conclude that even though the qualitative image of the different solutions is the same, notable differences exist in the evolutions and local behavior. These show that a refinement of the computational tools is necessary before we can hope to achieve accurate predictions. Moreover, additional comparisons to experimental results [11] are necessary to assess more complex solidification models that can describe the physics of solidification in more detail.

Acknowledgement

This work was funded by the French National Research Agency (ANR) in the framework of the

“Programme Blanc”, as part of the project SMACS (ANR-07-BLAN-190).

References

[1] Roache, P.J; Verification and Validation in Computational Science and Engineering Albuquerque, (NM), USA, Hermosa, (1998).

[2] Combeau, H.; Bellet, M. ; Fautrelle Y, ; Gobin, D. ; Rady, M.; Arquis, E; Budenkova, O. ; Dussoubs, B. ; Du Terrail Y., Kumar A., Gandin C.A., Goyeau B., Mosbah, S. ; Zaloznik, M. ; Benchmark sur la simulation des macroségrégations lors de la solidification d’un alliage : première synthèse. Actes du Congrès SFT (2010), pp. 493-498.

[3] Bellet, M. ; Combeau, H., Fautrelle, Y. ; Gobin, D. ; Rady, M. ; Arquis, E. ; Budenkova, O. ; Dussoubs, B. ; Duterrail, Y. ; Kumar, A. ; Gandin, C.A. ; Goyeau, B. ; Mosbah, S. ; Založnik, M.; Call for contributions to a numerical benchmark problem for 2D columnar solidification of binary alloys. *Int. J. Thermal Sciences,* 48 (11), (2009) pp 2013–2016.

[4] Liu, W.; *Finite element modelling of macrosegregation and thermomechanical phenomena in solidification processes*, PhD Thesis, Mines-ParisTech, (2005)

[5] Patankar, S., *Numerical Heat Transfer and Fluid Flow* (Hemisphere), (1980)

[6] FLUENT 6.2 User’s Guide, Fluent Inc. (2005).

[7] Ahmad, N.; Combeau, H.; Desbiolles, J.-L.; Jalanti, T.; Lesoult, G.; Rappaz, J.; Rappaz, M.; Stomp, C.; Numerical simulation of macro-segregation : a comparison between finite volume method and finite element method predictions and a confrontation with experiments, *Metall. Mater. Trans*., 29A, (1998), pp. 617-630.

[8] Thetis, Code de Mécanique des Fluides, http://thetis.enscpb.fr/ (2009)

[9] Rady, M.; Arquis, E.; Gobin, D.; Goyeau, B.; Numerical simulation of channel segregates during alloy solidification using TVD schemes, Int. J. of Numerical Methods for Heat and Fluid Flow, Vol. 20, n°8, (2010), pp. 841-866

[10] Voller, V.R.; Brent, A.; Prakash, C.; (1989), The modeling of heat, mass and solute transport in solidification systems, *Int. J. Heat Mass Transfer*, 32, 1719-1731.

[11] Hebditch, D. J.; Hunt, J. D.; (1974), Observations of ingot macrosegregation on model systems, *Metall. Trans*. 5 1557-1564.

[12] Combeau, H.; Bellet, M. ; Fautrelle, Y.; Gobin, D.; Arquis, E. ; Budenkova, O.; Dussoubs, B.; Duterrail, Y.; Kumar, A; Mosbah, S; Quatravaux T. ; Rady, M.; Gandin, C.-A.; Goyeau, B.; Založnik, M.; A Numerical benchmark on the prediction of macrosegregation in binary alloys, Proceeding of , TMS Ed. (2010)